Effect of magnetic Gd impurities on the superconducting state of amorphous Mo-Ge thin films with different thickness and morphology

Hyunjeong Kim, Anil Ghimire, Shirin Jamali, Thaddee K. Djidjou, Jordan M. Gerton, and A. Rogachev
Department of Physics and Astronomy, University of Utah, Salt Lake City, Utah 84112, USA
(Received 20 August 2011; revised manuscript received 1 February 2012; published 18 July 2012)

We studied the effect of magnetic doping with Gd atoms on the superconducting properties of amorphous $Mo_{70}Ge_{30}$ films. We observed that in uniform films deposited on amorphous Ge, the pair-breaking strength per impurity strongly decreases with film thickness initially and saturates at a finite value in films with thickness below the spin-orbit scattering length. The variation is likely caused by surface-induced magnetic anisotropy and is consistent with the fermionic mechanism of superconductivity suppression. In thin films deposited on SiN the pair-breaking strength becomes zero. Possible reasons for this anomalous response are discussed. The morphological distinctions between the films of the two types were identified using atomic force microscopy with a carbon nanotube tip.

DOI: 10.1103/PhysRevB.86.024518 PACS number(s): 74.81.Bd, 74.40.Kb, 74.62.En

I. INTRODUCTION

Understanding physical processes related to localized magnetic moments is particularly important for low-dimensional systems since such moments can form spontaneously on surfaces and interfaces of nominally nonmagnetic materials. The formation of localized magnetic moments in semiconductor heterostructures and devices are known to be carried by structural defects with unpaired electrons.[1] Localized magnetic moments were recently detected on the surface of a normal metal;[2] in superconducting systems, they are believed to be responsible for several unusual effects such as $1/f$ noise in superconducting quantum interference devices (SQUIDs) and qubits[3] and an anomalous magnetic field enhancement of a critical current in nanowires.[4] The origin of spontaneously formed magnetic moments often remains unknown; on the other hand, their effects can be probed by magnetic moments that are introduced intentionally.

Here we study the effect of intentional magnetic doping on transport properties of ultrathin MoGe films that undergo a superconductor-insulator transition (SIT).[5–10] The mechanism of the SIT remains an important unresolved problem in condensed matter physics. In general, there are several distinct physical processes that may lead to the SIT. Within the fermionic mechanism, Cooper pairing is locally suppressed by disorder-enhanced electron-electron repulsion.[11,12] The fermionic theories predict that the pair-breaking strength of magnetic impurities does not change with increasing disorder or decreasing film thickness.[13,14] Experimentally, magnetic doping was studied in quench-condensed Pb[15] and Pb-Bi films.[16] In the latter case, behavior consistent with the fermionic theory was observed relatively far from the SIT. Several bosonic mechanisms were proposed for the critical regime of the SIT. In these models, Cooper pairs are preserved across the transition but coherence in the films is lost due to vortex proliferation,[17] disorder-induced Cooper pair localization,[18,19] or fluctuations of the superfluid order parameter.[20] While the models cited in Refs. 18–20 differ in their detailed microscopic mechanisms, they all predict the appearance of a spatially inhomogeneous superconducting state. The emergence of this state was observed in numerical simulations[21] and was recently detected experimentally.[22] Possible effects of magnetic pair-breaking within the bosonic models have not yet been analyzed theoretically.

The amorphous MoGe system is particularly suitable for studying magnetic doping. This is the only known system where suppression of the critical temperature can be explained by the fermionic theory in all range of films thicknesses. Moreover, this can be achieved with the constrained theory, which assumes that effective electron-phonon coupling is not affected by disorder or film thickness. MoGe films with this property need to be deposited on a substrate covered with an underlayer of amorphous Ge that helps to maintain constant bulk resistivity of the film and ensures its homogeneity.[23] On the other hand, a missing Ge underlayer makes it possible to obtain and test an inhomogeneous superconducting state. We selected Gd as a magnetic dopant because its magnetic moment is carried by a half-filled f shell and does not depend on the host material.

II. TRANSPORT PROPERTIES OF MO-GE-GD FILMS

The critical temperature of amorphous Mo_xGe_{100-x} alloys depends on the particular value of x. In the first stage of our study, we used cosputtering from three independently controlled guns with Mo, Ge, and Gd targets to fabricate a series of thick Mo_xGe_{100-x}-Gd films with varying Gd content and x in the range 50–80 at.%. From transport measurements on these films we found that the alloy with $x \simeq 70$ is the most suitable for the Gd doping. In this alloy the superconductivity is completely suppressed when 6.5 at.% of Gd is added; at lower Gd content we detected a single-step superconducting transition in $R(T)$ curves.

We fabricated two series of $Mo_{70}Ge_{30}$ films. Films of the A series were deposited on a Si substrate covered with a 60-nm-thick layer of SiN grown by chemical vacuum deposition. For the B series, prior to the deposition of MoGe film, a 3-nm-thick underlayer of amorphous Ge was deposited. For oxidation protection the films of both series were covered by a 3-nm-thick layer of Ge. In Fig. 1(a), we show the temperature dependence of the sheet resistance for undoped $Mo_{70}Ge_{30}$ films deposited on SiN (A series). Within the studied temperature range (down to 0.3 K) the system

 ©2012 American Physical Society

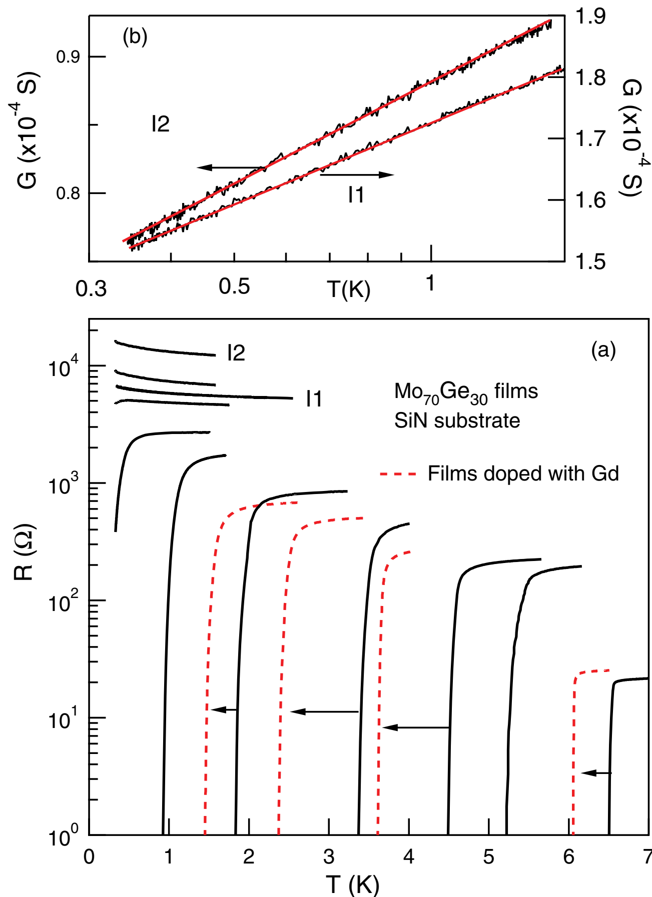

FIG. 1. (Color online) (a) Sheet resistance versus temperature for a series of amorphous $Mo_{70}Ge_{30}$ films deposited on SiN substrates (solid lines). The dashed lines indicate films doped with Gd; arrows indicate the correspondence between undoped and doped films. (b) Conductance of insulating films I1 and I2 as a function of temperature on a logarithmic scale. The solid red line is a linear fit.

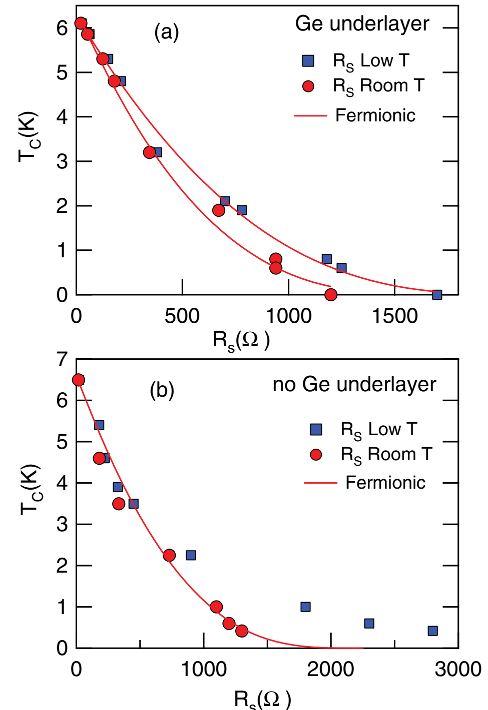

FIG. 2. (Color online) (a) Critical temperature versus sheet resistance at room and low temperature (just before the superconducting transition). The solid lines indicate fits to the fermionic theory. (b) Same data for the films deposited on SiN.

undergoes a direct SIT with no intermediate metallic phase. The data on the figure indicate that, with increasing sheet resistance R_S, the critical temperature progressively decreases and films with sufficiently high R_S become insulating. As shown in Fig. 1(b), in the insulating regime, conductance has a logarithmic temperature correction arising due to the weak localization and electron-electron interaction contributions. Qualitatively, similar suppression of superconductivity was observed for films deposited on a Ge underlayer (B series).

We define an empirical mean-field T_c at the middle of the superconducting transition. In Fig. 2(a) we plot this quantity for the B series of films deposited on Ge as a function of sheet resistance R_S at room temperature [$R_S(RT)$] and at low temperature [$R_S(LT)$]—just above the superconducting transition. We found that, regardless of what parameter is chosen, $R_S(RT)$ or $R_S(LT)$, the dependence of T_c can be well explained by the fermionic theory[11] as shown in the figure. For the fitting we used the formula[24]

$$\ln\left(\frac{T_c}{T_{c0}}\right) = \frac{1}{|\gamma|} - \frac{1}{2\sqrt{ut}} \ln \frac{1+\sqrt{ut}/|\gamma|}{1-\sqrt{ut}/|\gamma|}, \qquad (1)$$

where $u = 1/2$ and $t = [e^2/(2\pi^2\hbar)]R_S$. The best fit shown in the figure was obtained with the adjustable parameter $|\gamma| = 0.117$ for $R_S(LT)$ and $|\gamma| = 0.107$ for $R_S(RT)$. The question of which parameter $R_S(LT)$ or $R_S(RT)$ should be used for analysis has not been discussed theoretically. We notice that, in Ref. 11, the comparison with the fermionic model for $Mo_{78}Ge_{22}$ films was done using T_c versus $R_S(LT)$ dependence. Using the published data for this material[23] we verified that the theory works equally well if $R_S(RT)$ is used instead.

The behavior of T_c in A-type films shown in Fig. 2(b) is more interesting. The dependence of T_c on $R_S(RT)$ can be well explained by the fermionic theory. However, the dependence of T_c on the sheet resistance at low temperatures, $R_S(LT)$, deviates strongly from the theory for film thicknesses below 1.5 nm. The sheet resistance at room temperature is a good approximation for the Boltzmann resistance that is dominated by elastic scattering for MoGe alloys (mean-free path in MoGe is $\ell \approx 0.3$ nm[23]). The growth of resistance between 300 K and 4 K is due to quantum corrections that, for the A series, are significant and exceed 100% for the critical film. It is interesting to note that the critical sheet resistance of the A series at low temperature (≈5 kΩ) is close to the universal sheet resistance $R_q = h/(4e^2) = 6.45$ kΩ predicted within the "dirty boson" model.[17] The difference in the behavior of T_c in the A and B series cannot be explained by a change in the dielectric constant of the substrate. SiN has a lower dielectric constant than α-Ge; therefore, electron-electron interactions in the A-series films have weaker screening and suppression of T_c would be expected at lower values of sheet resistance than in the B series.

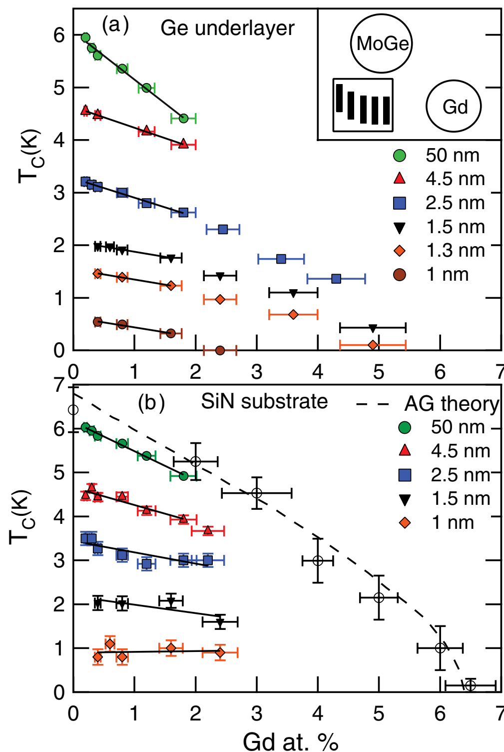

FIG. 3. (Color online) (a) Critical temperature versus Gd content for films with a Ge underlayer (B series). The inset indicates the arrangements of samples and targets in the sputtering chamber for two-gun cosputtering. (b) Critical temperature versus Gd content for films with indicated thickness deposited on the SiN substrates. The dashed line is a fit of the data in the extended Gd percentage range to the Abrikosov-Gor'kov theory.

The deviation from the fermionic theory in A-type films correlates with an anomalous behavior of thin MoGe films doped with Gd. The inset to Fig. 3(a) shows an arrangement of samples and targets used for fabrication of these films. The deposition was carried out by cosputtering from two guns. Several substrates were positioned approximately at the same distance from the composite MoGe target, but at varying distances from the Gd target. For each position, the deposition rate was calibrated by profile measurement of a test thick film; the thickness of films was controlled by the deposition time. Films within each series were fabricated in the same run under the same vacuum and deposition conditions. They have the same thickness but systematically varying Gd content.

The temperature dependence of sheet resistance for several representative Gd-doped films is shown as dashed lines in Fig. 1(a). The magnetic doping simply shifts the superconducting transition, leaving its width and normal state resistance essentially unchanged. Figure 3 displays the critical temperature versus Gd content. Uncertainties in the Gd content originate from the deposition time, deposition rate and positioning of the sample holder inside of the chamber. We found that thin A-type films with the same nominal thickness deposited in the same run revealed random variations in T_c. The uncertainty in T_c resulting from this effect is indicated by vertical error bars in Fig. 3(b). It was estimated from measurements on several series of undoped films deposited under the same conditions as the doped ones. It is interesting to note that this effect was not detected in the B-type films deposited on Ge. In A-type films, a deviation of T_c from the average value was always accompanied by a concurrent change in the $R_S(LT)$ of a film; in fact, we found no uncertainty in T_c vs $R_s(LT)$ relation.

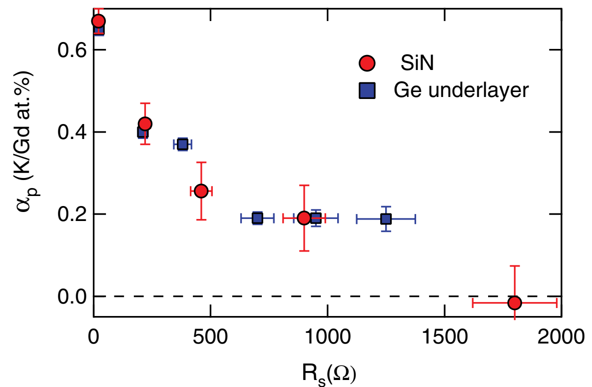

FIG. 4. (Color online) Pair-breaking strength per impurity, α_p, as a function of the film resistance at low temperatures for films deposited on SiN and amorphous Ge.

In Fig. 3(b), the open circles show the dependence of T_c on Gd content for thick MoGe films fabricated by three-gun (Mo, Ge, and Gd) deposition in the extended range of doping. The data can be fit with the Abrikosov-Gor'kov (AG) theory.[25] The critical concentration of Gd is 6.5 at.%; the corresponding volume critical concentration is $n_c = 3 \times 10^{21}$ cm^{-3}. The rest of the data were obtained with the two-gun deposition. The AG theory predicts that, at low doping, T_c behaves as $k_B(T_{c0} - T_c) = \pi\alpha/4$. The total pair-breaking strength α is related to the pair-breaking strength per impurity as $\alpha = \alpha_p n_p$, where n_p is the concentration of impurities. A linear suppression of T_c is expected and indeed was observed experimentally. The parameter α_p computed from the linear fit to the data is plotted as a function of the film resistance in Fig. 4.

For MoGe films deposited on Ge, we found that with decreasing film thickness the pair-breaking strength drops initially by about a factor of three and then saturates for films with thickness below 1.5 nm. From the fermionic theories we expect that $\alpha_p \approx$ const; however, this conclusion is made under the assumption that the exchange coupling between a localized spin and conduction electrons does not change with decreasing film thickness or increasing disorder.

The behavior of α_p in MoGe films appears to be qualitatively similar to the reduction of the Kondo contribution in thin films of normal metals doped with magnetic atoms.[26] Extensive studies of this effect revealed that it is stronger for impurities with integer spin[27] and depends on surface roughness.[28] The effect was explained in terms of spin-orbit–induced magnetic anisotropy for magnetic impurities in proximity to the film surface.[29] The theory predicts that, close to the surface, the effective spin of a magnetic impurity is reduced.

Both the Kondo effect and magnetic pair breaking depend on total impurity spin and exchange interaction between this spin and conduction electrons. From the known diffusion coefficient $D = 0.5$ cm^2/s[23] and spin-orbit scattering time $\tau_{so} = 5 \times 10^{-14}$ s[30] we can estimate the average spin-orbit scattering length in MoGe as $\ell_{so} = \sqrt{D\tau_{so}} \approx 1.6$ nm.

Experimentally, this value of ℓ_{so} coincides with the film thickness below which the saturation of α_p takes place. This observation suggests that the pair-breaking strength of a Gd atom is reduced when it is located within ℓ_{so} from the surface of a film; the growth of α_p in thicker films corresponds to the increasing fraction of Gd atoms with a bulk-like surrounding. In other words, we have a gradual transition from anisotropic to isotropic exchange.

For MoGe films deposited on Ge, we always found that the suppression of superconductivity by magnetic impurities and thickness reduction are additive processes. A magnetic impurity introduced into a superconductor suppresses the order parameter locally.[31] The local suppression of the order parameter with decreasing film thickness is also a feature of the fermionic mechanism of the SIT. In this regard, the additivity of the two processes even very close to the critical point of the SIT is consistent with the fermionic mechanism of superconductivity suppression. Moreover, the $\alpha_p \approx$ const. relation that we found in our thinnest films agrees with the specific prediction made within the fermionic model.

Let us now discuss how magnetic doping affects thin A-type films. As shown in Fig. 4(b), in the film with nominal thickness of 1 nm, the pair-breaking strength at low doping becomes zero; adding magnetic impurities to the film does not change its T_c. One possibility for this anomalous response is that the spin-orbit–induced magnetic anisotropy gets stronger in films deposited on SiN because it has a larger semiconductor gap. It is also possible that the anomalous response to the magnetic doping is related to the distinct morphology of the thin A-type films, which may result in an inhomogeneous superconducting state.

III. MORPHOLOGY OF FILMS

Looking for a possible structural origin for the different behavior of thin films with and without a Ge underlayer, we inspected the surface morphology of several test samples using an atomic force microscope (AFM). A single-walled carbon nanotube was attached to the AFM probe,[32,33] which increased its lateral resolution to ~2 nm. Figure 5 shows typical AFM images of the two types of SiN substrates used in this work: Fig. 5(a) shows a bare SiN substrate (type A) and Fig. 5(b) shows a SiN substrate coated with a 3-nm-thick layer of Ge (type B). These AFM images were acquired under ambient conditions immediately after deposition and are both plotted using the same false-color scale to encode the topographical height variations. Visual inspection of these AFM images reveals some subtle morphological differences; primarily, it seems that the bare SiN substrate [Fig. 5(a)] has more pits than bumps, while the Ge-covered substrate has roughly equal proportions of both. Importantly, the topographical height variations for both the bare and Ge-coated substrates are similar (rms roughness ~400 pm for both), so the Ge layer does not seem to contribute to roughness on the samples.

Figure 6 shows typical AFM images of MoGe films of nominal thickness 1.5 nm on the two types of substrates: on a bare SiN substrate (type A) in Fig. 6(a) and on a Ge-coated substrate (type B) in Fig. 6(b). In both cases, the MoGe films were covered by a 1 nm layer of Ge for oxidation protection. Three-dimensional (3D) renderings of

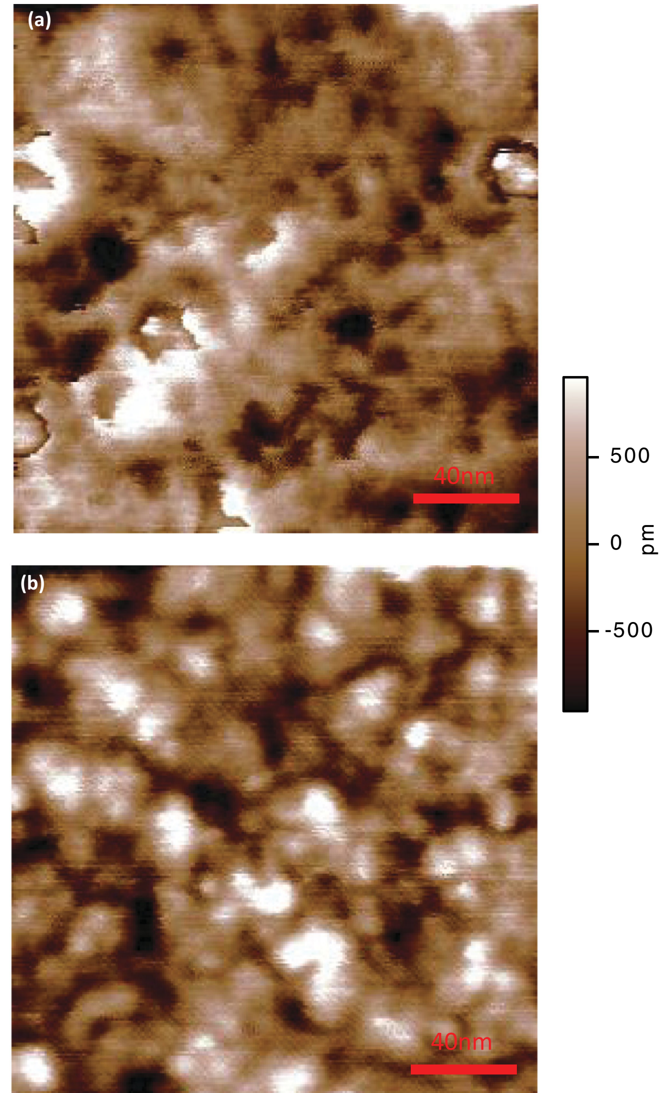

FIG. 5. (Color online) (a) Two-dimensional (2D) AFM image of bare SiN substrate. (b) 2D AFM image of SiN substrate coated with 3-nm-thick Ge layer. Size of the images is 200 × 200 nm^2.

AFM images taken from different spots on the same films are shown in Fig. 7. Visual inspection of these four images reveals clear morphological differences between the two types of film: the MoGe film on the type-A substrate has smaller lateral features whereas that on the type-B substrate is smoother. Overall, we made several different measurements of MoGe films and observed that those on type-A substrates had on average smaller islands and sharper boundaries between them. These morphological differences seem to be related to the lateral feature sizes only as again the topographical height variations are similar for both types of films (rms roughness ~500 pm for both).

To extract quantitative information about the lateral scale of the topographical features, a spatial Fourier transform was performed on the AFM data. To reduce noise, the resulting data were averaged over different directions in Fourier space, yielding a one-dimensional (1D) profile of the amplitude of height variations as a function of the spatial Fourier frequency k for both type-A and type-B samples [Fig. 8(a)]. In Fig. 8(b)

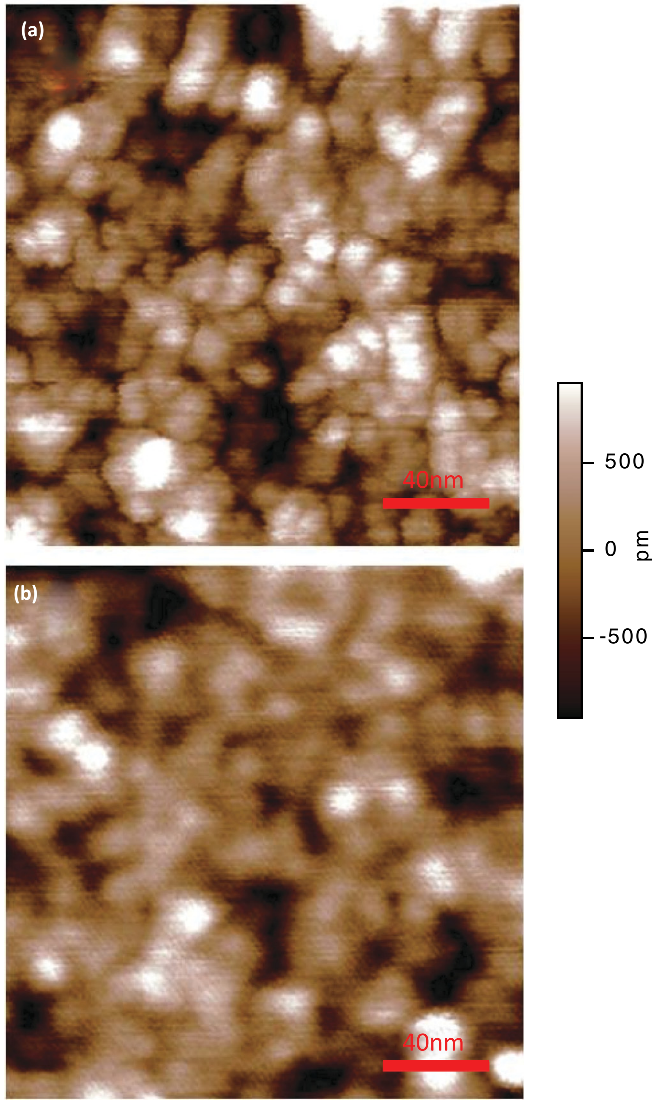

FIG. 6. (Color online) (a) Two-dimensional (2D) AFM image of the surface of 1.5-nm-thick MoGe film deposited on bare SiN (type A). (b) 2D AFM image of a similar film deposited on SiN covered with 3-nm-thick Ge underlayer (type B). Both films were covered with 1-nm-thick protective Ge overlayer. Size of the images is 200×200 nm^2.

we show the difference between the 1D Fourier profiles of the type-A and type-B films shown in Figs. 7(a) and 7(b), respectively, normalized to their average profile. The overabundance of intermediate spatial frequencies for the type-A sample indicates that the Ge underlayer smoothes the surface and suppresses topographical features with a characteristic lateral scale of about 15 nm.

Morphological differences between MoGe films on the two types of substrate can also be characterized using a height-height correlation function,

$$H_x(\tau_x) = \frac{1}{N(M-m)} \sum_{l=1}^{N} \sum_{n=1}^{M-m} (z_{n+m,l} - z_{n,l})^2, \quad (2)$$

where $\tau_x = x_1 - x_2$ is the distance between two points in the same horizontal row of the image, $m = \tau_x/\Delta x$ is the number of pixels of size Δx between the two points, N is the number of rows in the image, M is the number of columns, and $z_{\alpha,\beta}$ is

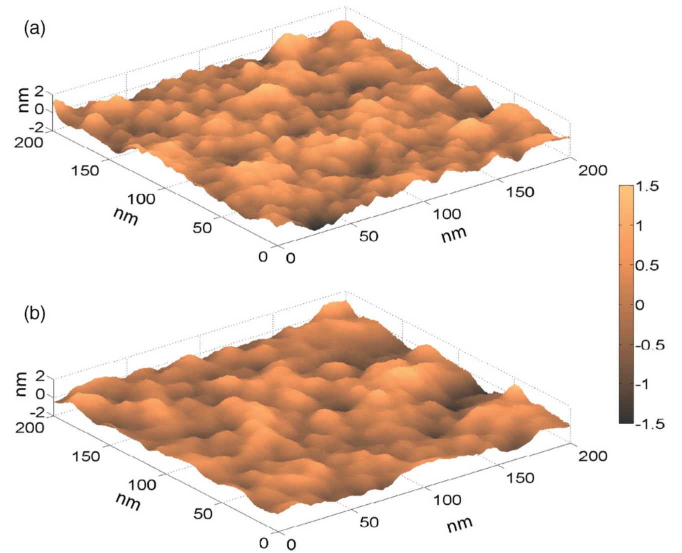

FIG. 7. (Color online) (a) 3D AFM image of the surface of 1.5-nm-thick MoGe film deposited on bare SiN (type A). (b) 3D AFM image of a similar film deposited on SiN covered with 3-nm-thick Ge underlayer (type B). Both films were covered with 1-nm-thick protective Ge overlayer.

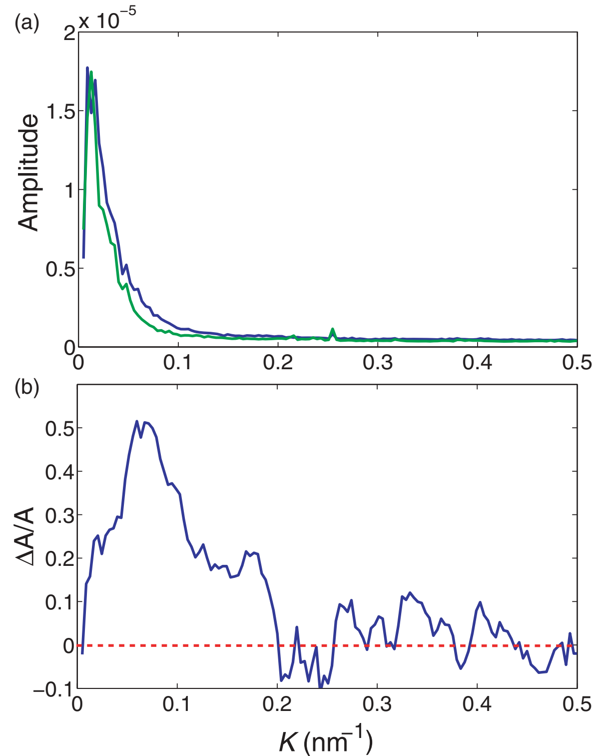

FIG. 8. (Color online) Spatial Fourier analysis of AFM images for MoGe films deposited on type-A and type-B substrates. (a) Fourier amplitude as a function of the spatial frequency K for films deposited on a bare SiN substrate (upper, blue trace) and a Ge underlayer (lower, green trace). (b) The difference ΔA between the 1D Fourier profiles of the type-A and type-B films shown in panel (a), normalized to the average A of the two profiles.

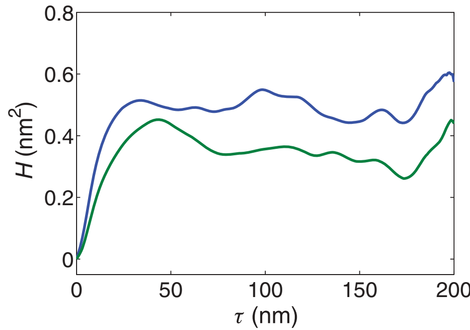

FIG. 9. (Color online) Height-height correlation plots for MoGe films deposited on a bare SiN substrate (upper blue trace) and a Ge underlayer (lower green trace).

the topographical height at column α and row β. H_x provides a measure of the horizontal distance between points for which their respective topographical heights become uncorrelated. In particular, for points on the sample that are very close together (small τ_x), their heights should be strongly correlated, so H_x should be near zero; for larger separations, one would expect less correlation so H_x will increase. If the sample morphology is completely random, H_x should saturate at a value that reflects the rms roughness of the sample.

Note that an analogous expression to that in Eq. (2) can be written for the height-height correlation function $H_y(\tau_y)$, which corresponds to exchanging all the rows and columns of the image. Since our samples are isotropic in the x-y plane, we averaged $H_x(\tau_x)$ and $H_y(\tau_y)$ to obtain $H(\tau)$. This is plotted in Fig. 9 for the type-A (blue curve) and type-B (green curve) MoGe films corresponding to those shown in Fig. 7. Clearly, height correlations persist to larger values of τ for the type-B film (with Ge under layer) compared to the type-A film (bare SiN), which is consistent with both the Fourier analysis shown in Fig. 8 and the AFM images in Figs. 6 and 7. Interestingly, there appears to be some long-range order in the films, as indicated by the smaller features in the correlation function at larger values of τ [a completely random topography would exhibit a flat trace of $H(\tau)$ at large τ]. Currently, we have no explanation for the existence of such long-range order.

Evidently, the absence of a Ge underlayer introduces inhomogeneities that lead to important morphological differences compared to the Ge-undercoated films, but that are not strong enough to form a disconnected granular structure. This is also evident from transport measurements; Fig. 1(a) shows that even for the thinnest films, the superconducting transition remains sharp with a well defined T_c. There is no tail in $R(T)$ as it is typically observed in granular materials.[34] Normal state properties of the films also do not indicate the presence of strong inhomogeneities. From the theory of weak localization (Eq. 4.47a in Ref. 35) we estimated that the dephasing length L_φ at $T = 0.3$ K is about 80 nm for our least resistive insulating film. Since we do not see any sign of insulating behavior down to $T = 0.3$ K, the one-electron localization length in our films should be larger (probably much larger) than 80 nm and thus cover many random "hills" and "valleys" of the films' morphological profile.

IV. SUMMARY

In summary, we have studied the effect of magnetic doping on superconducting $Mo_{70}Ge_{30}$ films. For uniform films deposited on amorphous Ge, the suppression of superconductivity is consistent with the fermionic mechanism. In thin films deposited on bare SiN, the pair-breaking strength approaches zero. It is possible that the anomalous response to magnetic doping in films deposited on bare SiN is related to differences in film morphology, in particular to the formation of lateral features of smaller size. These morphological differences may in turn lead to the formation of an inhomogeneous superconducting state. Spatial nonuniformity of the order parameter is a common ingredient of bosonic models. Analysis of the effect of magnetic impurities within these models can perhaps explain our findings.

ACKNOWLEDGMENTS

We thank L. N. Bulaevskii, A. M. Finkel'stein, P. M. Goldbart, L. Ioffe, A. Kapitulnik, G. Refael, and B. Spivak for discussions and valuable comments. This work is supported by NSF CAREER Grant DMR-0955484 (A.R.) and NSF CAREER Grant DBI-0845193 (J.M.G.).

[1]E. H. Poindexter, *Semiconductor Interfaces, Microstructure, and Devices*, edited by Z. C. Feng, Chap. 10 (Inst. Phys. Publ., Bristol, Philadelphia, 1993).
[2]H. Bluhm, J. A. Bert, N. C. Koshnick, M. E. Huber, and K. A. Moler, Phys. Rev. Lett. **103**, 026805 (2009).
[3]S. Sendelbach, D. Hover, A. Kittel, M. Mück, J. M. Martinis, and R. McDermott, Phys. Rev. Lett. **100**, 227006 (2008); L. Faoro and L. B. Ioffe, *ibid.* **100**, 227005 (2008); S. K. Choi, D.-H. Lee, S. G. Louie, and J. Clarke, *ibid.* **103**, 197001 (2009); F. Yoshihara, Y. Nakamura, and J. S. Tsai, Phys. Rev. B **81**, 132502 (2010).
[4]A. Rogachev, T.-C. Wei, D. Pekker, A. T. Bollinger, P. M. Goldbart, and A. Bezryadin, Phys. Rev. Lett. **97**, 137001 (2006).
[5]D. B. Haviland, Y. Liu, and A. M. Goldman, Phys. Rev. Lett. **62**, 2180 (1989).
[6]N. Markovic, C. Christiansen, and A. M. Goldman, Phys. Rev. Lett. **81**, 5217 (1998).
[7]V. F. Gantmakher, M. V. Golubkov, V. T. Dolgopolov, G. E. Tsydynzhapov, and A. A. Shashkin, JETP Lett. **68**, 363 (1998).
[8]G. Sambandamurthy, L. W. Engel, A. Johansson, and D. Shahar, Phys. Rev. Lett. **92**, 107005 (2004).
[9]T. I. Baturina, A. Yu. Mironov, V. M. Vinokur, M. R. Baklanov, and C. Strunk, Phys. Rev. Lett. **99**, 257003 (2007).
[10]M. A. Steiner, N. P. Breznay, and A. Kapitulnik, Phys. Rev. B **77**, 212501 (2008).
[11]A. M. Finkel'stein, JETP Lett. **45**, 46 (1987).
[12]T. R. Kirkpatrick and D. Belitz, Phys. Rev. Lett. **68**, 3232 (1992).
[13]T. P. Devereaux and D. Belitz, Phys. Rev. B **53**, 359 (1996).
[14]R. A. Smith and V. Ambegaokar, Phys. Rev. B **62**, 5913 (2000).

[15] J. S. Parker, D. E. Read, A. Kumar, and P. Xiong, Europhys. Lett. **75**, 950 (2006).
[16] J. A. Chervenak and J. M. Valles Jr., Phys. Rev. **51**, 11977 (1995).
[17] M. P. A. Fisher, Phys. Rev. Lett. **65**, 923 (1990).
[18] M. V. Feigel'man, L. B. Ioffe, V. E. Kravtsov, and E. A. Yuzbashyan, Phys. Rev. Lett. **98**, 027001 (2007).
[19] V. L. Pokrovsky, G. M. Falco, and T. Nattermann, Phys. Rev. Lett. **105**, 267001 (2010).
[20] B. I. Spivak and S. A. Kivelson, Phys. Rev. B **43**, 3740 (1991).
[21] A. Ghosal, M. Randeria, and N. Trivedi, Phys. Rev. B **65**, 014501 (2001).
[22] B. Sacepe, C. Chapelier, T. I. Baturina, V. M. Vinokur, M. R. Baklanov, and M. Sanquer, Phys. Rev. Lett. **101**, 157006 (2008); B. Sacepe *et al*., Nat. Phys. **7**, 239 (2011).
[23] J. M. Greybeal, Ph.D. thesis, Stanford University (1985).
[24] Y. Oreg and A. M. Finkel'stein, Phys. Rev. Lett. **83**, 191 (1999).
[25] A. A. Abrikosov and L.P. Gor'kov, Sov. Phys. JETP **15**, 752 (1962).
[26] G. Chen and N. Giordano, Phys. Rev. Lett. **66**, 209 (1991); J. F. DiTusa, K. Lin, M. Park, M. S. Isaacson, and J. M. Parpia, *ibid*. **68**, 1156 (1992).
[27] T. M. Jacobs and N. Giordano, Europhys. Lett. **44**, 74 (1998).
[28] V. Chandrasekhar, P. Santhanam, N. A. Penebre, R. A. Webb, H. Vloeberghs, C. Van Haesendonck, and Y. Bruynseraede, Phys. Rev. Lett. **72**, 2053 (1994); N. Giordano and T. M. Jacobs, J. Appl. Phys. **87**, 6079 (2000).
[29] O. Újsághy, A. Zawadowski, and B. L. Gyorffy, Phys. Rev. Lett. **76**, 2378 (1996).
[30] A. Rogachev, A. T. Bollinger, and A. Bezryadin, Phys. Rev. Lett. **94**, 017004 (2005).
[31] A. V. Balatsky, I. Vekhter, and J.-X. Zhu, Rev. Mod. Phys. **78**, 373 (2006).
[32] J. Hafner, C. Cheung, T. Oosterkamp, and C. J. Lieber, Phys. Chem. B **105**, 743 (2001).
[33] C. Mu, B. D. Mangum, C. Xie, and J. M. Gerton, IEEE J. Sel. Top. Quantum Electron. **14**, 206 (2008).
[34] A. V. Herzog, P. Xiong, F. Sharifi, and R. C. Dynes, Phys. Rev. Lett. **76**, 688 (1996).
[35] B. L. Altshuler and A. G. Aronov, in *Electron-Electron Interaction in Disordered Systems*, edited by A. L. Efros and M. Pollak (Elseveir Science Publ., Amsterdam, 1985).